Estimation of Kinetic Parameters Without Input Functions: Analysis of Three Methods for Multichannel Blind Identification

Dmitri Y. Riabkov* and Edward V. R. Di Bella

***Abstract*—Compartment modeling of dynamic medical image data implies that the concentration of the tracer over time in a particular region of the organ of interest is well modeled as a convolution of the tissue response with the tracer concentration in the blood stream. The tissue response is different for different tissues while the blood input is assumed to be the same for different tissues. The kinetic parameters characterizing the tissue responses can be estimated by multichannel blind identification methods. These algorithms use the simultaneous measurements of concentration in separate regions of the organ; if the regions have different responses, the measurement of the blood input function may not be required. Three blind identification algorithms are analyzed here to assess their utility in medical imaging: eigenvector-based algorithm for multichannel blind deconvolution; cross relations; and iterative quadratic maximum-likelihood (IQML). Comparisons of accuracy with conventional (not blind) identification techniques where the blood input is known are made as well. Tissue responses corresponding to a physiological two-compartment model are primarily considered. The statistical accuracies of estimation for the three methods are evaluated and compared for multiple parameter sets. The results show that IQML gives more accurate estimates than the other two blind identification methods.**

***Index Terms*—Blind identification, blood input, IQML, perfusion, physiological compartment model, tissue response.**

I. Introduction

In DYNAMIC imaging, for example with positron emission tomography (PET), single photon emission computed tomography (SPECT), or magnetic resonance imaging (MRI), a sequence of images over time can be acquired to track the regional uptake and washout of a radioactive or paramagnetic "tracer." Knowledge of the exchange rates of the tracer between blood and tissue is of clinical use in the diagnosis of disease. A standard method of processing the data involves drawing regions of interest (ROIs) on the images. These regions are associated with changes in tracer concentration over time (Fig. 1).

The measured concentration of the tracer in the tissue, here referred to as tissue time-concentration curves (TCs), can often be well modeled as the concentration of the tracer in the blood (blood input function) convolved with a regional tissue response

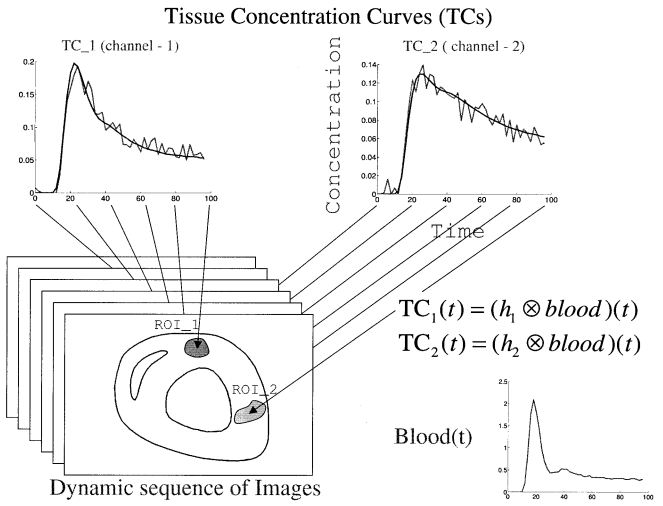

Fig. 1. Tissue time concentration curves measurement given by dynamic sequence of images.

[1]

$$x^{(i)}(t) = \left(h^{(i)} \otimes blood\right)(t) + \varepsilon^{(i)}(t) \tag{1}$$

where $x^{(i)}$ is the tissue time-concentration curve, $h^{(i)}$ is the tissue response for the tissue region designated by i, and $\varepsilon^{(i)}(t)$ is the noise due to the measurement process.

With certain assumptions, a physiological two-compartment model fits the data acquired with dynamic PET and SPECT imaging of certain tracers (for example, 99mTc-teboroxime) [2] and also can fit dynamic MRI of extracellular gadolinium (Gd)-based contrast agents [1]. For such a two-compartment model, the tissue impulse response is given by

$$h^{(i)}(t) = k_I^{(i)} \cdot e^{-t \cdot k_O^{(i)}} \tag{2}$$

where k_I is the washin rate constant (uptake) and k_O is the washout rate constant. These tissue kinetic parameters, k_I and k_O, provide diagnostic clinical information such as regional blood flow and distribution volume. The estimation of the kinetic parameters requires knowledge of the blood input function to solve (1). Although the input function can be estimated from the cardiac blood pool or an artery in the image data for some applications, the estimate is inaccurate in many cases. In PET and SPECT imaging, the estimate is inaccurate because the images may not reflect the amount of tracer available to the tissues. For example, some of the visible tracer may be bound to red blood cells and not extractable by the tissue. In MRI imaging, the es-

Manuscript received October 23, 2001; revised June 21, 2002. *Asterisk indicates corresponding author.*

*D. Y. Riabkov is with the Department of Physics, The University of Utah, 115 S, 1400 E, Salt Lake City, UT 84112 USA (e-mail: riabkov@physics.utah.edu).

E. V. R. Di Bella is with the Department of Radiology, The University of Utah, Salt Lake City, UT 84108 USA.

Digital Object Identifier 10.1109/TBME.2002.804588

timate may be inaccurate because of the nonlinear relationship between signal intensity and high Gd concentrations; the compartment model is based on Gd concentrations rather than signal intensities.

It is often possible to obtain accurate input functions by direct arterial blood sampling. However, this method poses health risks and is complicated and may require additional medical personnel. Other approaches have been formulated to use a limited number of venous samples [3] or population-based approaches [4] to obtain an accurate input function. Very little work has been done to estimate kinetic parameters without any blood samples and with no knowledge of the population. A noninvasive approach based on the cross relations (CR) blind channel estimation method was used in [2] to estimate the kinetic parameters without any knowledge of the blood input. A similar method, eigenvector based algorithm for multichannel blind deconvolution (EVAM) [5], was used to estimate the parameters of a three compartment model for PET FDG imaging [6]. Other approaches in which both the blood input and kinetic parameters are treated as unknowns have been explored [7]–[9]. No work has yet been presented on the application of the iterative quadratic maximum-likelihood method (IQML) to parameter estimation in medical imaging. The blind identification problem can be treated as a nonlinear least squares problem whose variables are separate [10]. IQML promises a more optimal solution by using this property.

II. Blind Identification Problem in Two-Compartment Models

Assuming that the measurements of tissue concentration curves at times $t = \Delta t \cdot n$ ($n = 0, \ldots, N-1$) from p regions of interest (channels) with different kinetics are performed it is possible to write the following system of equations:

$$\begin{cases} x^{(1)}(n) = \left(h^{(1)} \otimes b\right)(n) \\ \cdots \\ x^{(p)}(n) = \left(h^{(p)} \otimes b\right)(n) \end{cases} \tag{3}$$

where $b(n)$ is blood input function and

$$h^{(i)}(n) = k_I^{(i)} \cdot \Delta t \cdot e^{-n \cdot \Delta t \cdot k_O^{(i)}}. \tag{4}$$

Multichannel blind identification algorithms can be applied to solve this system for parameters $k_I^{(i)}$ and $k_O^{(i)}$ (here, $i = 1, \ldots, p$) in tissue responses $h^{(i)}(n)$ without knowing $b(n)$. Note that the parameters $k_I^{(i)}$ can be found only within a scale factor (as ratios). (k_I and k_O often vary approximately 20% in normal tissue and up to 400% in disease.) To solve this system of equations, we also assume that the following condition is satisfied: the transfer functions $h^{(i)}(n)$ for different channels should not have any common zeros or poles [5]. This means that for the tissue response of (2) that all of the washout rate constants, $k_O^{(i)}$, should be different.

A. Uniqueness

The question of uniqueness of the solution is whether only one set of the coefficients k_I and k_O and input function $b(n)$ corresponds to the set of $x^{(i)}(n)$. Using the results in [5] in the framework of the EVAM algorithm, we can show that the solution is unique for the two-compartment model in (2), within a global scale factor. A proof of uniqueness is shown in the Appendix-A.

B. Noise

In practice, the measured tissue concentration curves always have noise. A small amount of noise can cause significant errors in estimates of tissue parameters. Also, different estimation algorithms can give different estimates for noisy data. In this regard, we made estimations of k_I and k_O from simulated noisy tissue concentration curves using the three different multichannel blind identification methods. Cardiac MRI was chosen as the focus of these simulations so white Gaussian noise was used which is the appropriate noise model.

III. Description of the Three Methods for Multichannel Blind Identification

A. Cross Relations Method (CR)

The CR method is based on the fact that

$$\left[h^{(1)} \otimes b\right] \otimes h^{(2)} = h^{(1)} \otimes \left[b \otimes h^{(2)}\right] \tag{5}$$

$$x^{(1)} \otimes h^{(2)} \cong h^{(1)} \otimes x^{(2)}. \tag{6}$$

Equality is approximate because of the noise in the TCs. Minimizing the mean square error

$$\sum_{i=1}^{p-1} \sum_{j=i+1}^{p} \left\| x^{(i)} \otimes h^{(j)} - h^{(i)} \otimes x^{(j)} \right\|^2 \tag{7}$$

we can solve the system for the set of parameters $\{k_I^{(i)}, k_O^{(i)}\}$ (here, p is the number of channels). More description can be found in [2].

B. Iterative Quadratic Maximum-Likelihood (IQML)

The idea of this method has been adapted from the description in [11]. IQML was developed in [12], but the algorithm is related to the general foundation that appeared earlier in [10].

Since we have discrete measurements at times $t = \Delta t \cdot n$ ($n = 0, \ldots, N-1$), the expression

$$x^{(i)}(n) = \left(h^{(i)} \otimes b\right)(n) + \varepsilon^{(i)}(n) \tag{8}$$

can be written in terms of vectors as

$$\overrightarrow{x}^{(i)} = \mathbf{H}^{(i)} \overrightarrow{b} + \overrightarrow{\varepsilon}^{(i)} \tag{9}$$

where $\mathbf{H}^{(i)}$ is the convolution matrix of the tissue response for region i, $\overrightarrow{b}$ is the unknown blood vector, $\overrightarrow{x}^{(i)}$ and $\overrightarrow{\varepsilon}^{(i)}$ are the measured data and noise vectors for region i; correspondingly, ($\mathbf{H}^{(i)}$ is a nonsymmetric $N \times N$ Toeplitz matrix with first column $[h^{(i)}(0), \ldots, h^{(i)}(N-1)]^T$ and first row $[h^{(i)}(0), 0, \ldots, 0]$).

Stacking matrices on top of each other we can get a linear system of equations

$$\begin{bmatrix} \overrightarrow{x}^{(1)} \\ \vdots \\ \overrightarrow{x}^{(p)} \end{bmatrix} = \begin{bmatrix} \mathbf{H}^{(1)} \\ \vdots \\ \mathbf{H}^{(p)} \end{bmatrix} \overrightarrow{b} + \begin{bmatrix} \overrightarrow{\varepsilon}^{(1)} \\ \vdots \\ \overrightarrow{\varepsilon}^{(p)} \end{bmatrix} \tag{10}$$

which can be referred to in generalized form

$$\overrightarrow{\mathrm{TCS}} = \mathbf{H}\,\overrightarrow{b} + \overrightarrow{\varepsilon}. \tag{11}$$

Denoting $\mathbf{H}$ as $\tilde{\mathbf{H}}$ which is built using $\{\tilde{k}_I, \tilde{k}_O\}$, where $\tilde{k}_I$ and $\tilde{k}_O$ are the current estimates of the parameters $\{k_I, k_O\}$, the objective function then will be

$$R = \left\| \overrightarrow{\mathrm{TCS}} - \tilde{\mathbf{H}}\,\overrightarrow{\tilde{b}} \right\|^2 \tag{12}$$

which is minimized by varying $\{\tilde{k}_I, \tilde{k}_O\}$ and $\overrightarrow{\tilde{b}}$. This is a nonlinear least squares problem. But this problem can be simplified because for any fixed set of values $\{\tilde{k}_I, \tilde{k}_O\}$ it is easy to find the $\overrightarrow{\tilde{b}}$ that minimizes R [10]

$$\overrightarrow{\tilde{b}} = \tilde{\mathbf{H}}^{\dagger}\overrightarrow{\mathrm{TCS}}, \qquad \text{where } \tilde{\mathbf{H}}^{\dagger} = \left(\tilde{\mathbf{H}}^T\tilde{\mathbf{H}}\right)^{-1}\tilde{\mathbf{H}}^T. \tag{13}$$

Therefore

$$R = \left\| \left(\mathbf{I} - \tilde{\mathbf{H}}\tilde{\mathbf{H}}^{\dagger}\right)\overrightarrow{\mathrm{TCS}} \right\|^2 \tag{14}$$

is minimized just by varying $\{\tilde{k}_I, \tilde{k}_O\}$, which can be performed by any standard nonlinear minimization method. [In implementation, it is easier to use (13) and then (12) than it is to use (14) to calculate R. Also, the calculated $\overrightarrow{\tilde{b}}$ can be used in calculating the gradients of R (see the Appendix)].

C. Eigenvector-Based Algorithm for Multichannel Blind Deconvolution (EVAM)

Another approach is to use a system of finite-impulse response (FIR) filters to solve the blind deconvolution problem. The orders of the FIR filters of the blind deconvolution adaptive system [$\mathcal{W}^{(i)}$ in Fig. 2] are known because the physiological compartment model provides the form of the transfer function of the unknown system. Using this condition, the following is a simplified formulation of the full EVAM algorithm found in [5]. (The system is called adaptive because its filter coefficients will be varied to minimize an objective function; these coefficients can then be related to the unknown kinetic parameters.) A short description of the multichannel case is given in the Appendix.

The channels of the unknown system have unknown rational transfer functions $\mathcal{H}^{(i)}(z^{-1})$

$$\mathcal{H}^{(i)}(z^{-1}) = \frac{\mathcal{C}^{(i)}(z^{-1})}{\mathcal{D}^{(i)}(z^{-1})} \qquad i = 1, \ldots, p \tag{15}$$

where $\mathcal{C}^{(i)}(z^{-1})$ and $\mathcal{D}^{(i)}(z^{-1})$ are polynomials of orders $C^{(i)}$ and $D^{(i)}$ with unknown coefficients $c_0^{(i)}, \ldots, c_{C^{(i)}}^{(i)}$ and $d_0^{(i)}, \ldots, d_{D^{(i)}}^{(i)}$ correspondingly. With the tissue response of (2), the orders $C^{(i)} = 0$ and $D^{(i)} = 1$ and

$$\begin{aligned} \mathcal{C}^{(i)}(z^{-1}) &= c_0^{(i)}, \qquad i = 1, \ldots, p, \\ \mathcal{D}^{(i)}(z^{-1}) &= d_0^{(i)} + d_1^{(i)}z^{-1}. \end{aligned} \tag{16}$$

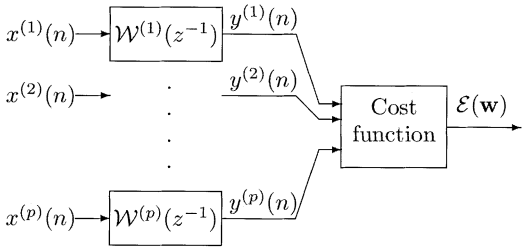

Fig. 2. Multichannel blind deconvolution framework: Adaptive system model. See text for details.

The blind deconvolution adaptive system consists of the same number of channels as the unknown system. Each channel consists of an FIR filter that takes the corresponding output from the unknown system as input (Fig. 2).

The transfer functions of the channels of the adaptive system are FIR filters

$$\mathcal{W}^{(i)}(z^{-1}) = w_0^{(i)} + w_1^{(i)}z^{-1} + \cdots + w_{W^{(i)}}^{(i)}z^{-W^{(i)}} \qquad i = 1, \ldots, p \tag{17}$$

which are polynomials of order $W^{(i)}$. If the vectors of coefficients are defined as

$$\mathbf{w}^{(i)} = \left[w_0^{(i)}, w_1^{(i)}, \ldots, w_{W^{(i)}}^{(i)}\right]^T \tag{18}$$

and the vectors of signals are defined as

$$\mathbf{x}^{(i)}(n) = \left[x^{(i)}(n), x^{(i)}(n-1), \ldots, x^{(i)}\left(n - W^{(i)}\right)\right]^T \tag{19}$$

then, the output signals for the channels of the adaptive system can be written as

$$y^{(i)}(n) = \mathbf{w}^{(i)T}\,\mathbf{x}^{(i)}(n). \tag{20}$$

The output signals of each channel of the adaptive system $y^{(i)}(n)$ then are used to produce the cost function $\mathcal{E}(\mathbf{w})$ [in the two channel case $\mathcal{E}(\mathbf{w}) = \sum_n (y^{(1)}(n) - y^{(2)}(n))^2$] which is minimized.

1) Two Channel Case: If we assume a noise free two-channel case the minimum of the cost function is reached when

$$\mathcal{H}^{(1)}\mathcal{W}^{(1)} - \mathcal{H}^{(2)}\mathcal{W}^{(2)} = 0. \tag{21}$$

Denoting the roots of the polynomials $\mathcal{D}^{(i)}$ as $\eta^{(i)}$

$$\frac{\rho_1}{\left(z^{-1} - \eta_1^{(1)}\right)}\mathcal{W}^{(1)}(z^{-1}) - \frac{\rho_2}{\left(z^{-1} - \eta_1^{(2)}\right)}\mathcal{W}^{(2)}(z^{-1}) = 0 \tag{22}$$

where $\rho_i = c_0^{(i)}/d_1^{(i)}$. Also, assuming

$$W^{(1)} = D^{(1)} + C^{(2)}, \quad W^{(2)} = D^{(2)} + C^{(1)} \tag{23}$$

it is possible to see that because there are no common zeros or poles between the channels transfer functions (due to the assumed condition in Section II), the only solutions for $\mathcal{W}^{(1)}(z^{-1})$ and $\mathcal{W}^{(2)}(z^{-1})$ which minimize $\mathcal{E}(\mathbf{w})$ will be

$$\mathcal{W}^{(i)}(z^{-1}) = \alpha \mathcal{D}^{(i)}(z^{-1}) c_0^{(j)}, \qquad i = 1, 2,\ j = 2, 1 \quad (24)$$

where α is an arbitrary constant. The orders of the FIR filters of the blind deconvolution adaptive system are known and equal for a physiological model of tissue response; $W^{(1)} = W^{(2)} = M$ where M is known ($M = 1$ in the two-compartment model case).

Defining the vector $\mathbf{w}$ of coefficients for a pair of channels

$$\mathbf{w} = \left[\mathbf{w}^{(1)T}, \mathbf{w}^{(2)T}\right]^T$$

the cost function can then be written as

$$\mathcal{E}(\mathbf{w}) = \mathbf{w}^T \mathbf{R} \mathbf{w} \quad (25)$$

where matrix $\mathbf{R}$ is

$$\mathbf{R} = \begin{bmatrix} \mathbf{R}_{1,1} & -\mathbf{R}_{1,2} \\ -\mathbf{R}_{2,1} & \mathbf{R}_{2,2} \end{bmatrix} \quad (26)$$

and the block matrices are defined as

$$\mathbf{R}_{i,j} = \sum_{n=M}^{N} \mathbf{x}^{(i)}(n) \mathbf{x}^{(j)T}(n). \quad (27)$$

It can be seen from (25) that the $\mathbf{w}$ which minimizes $\mathcal{E}(\mathbf{w})$ is the eigenvector of $\mathbf{R}$ corresponding to the minimal eigenvalue. In the presence of noise, this is also true [5]. Thus, the kinetic parameters of the tissue regions can be obtained using $\mathbf{w}$ [see (37) and (38) in the Appendix].

IV. Estimation With Known Blood Input (KBI)

Estimation of kinetic parameters using a known blood input function was considered in order to compare the multichannel blind identification methods with the ideal case. In this case, the blood input vector $\overrightarrow{b}$ is assumed to be known and for each channel the cost function

$$e^{(i)}\left(k_I^{(i)}, k_O^{(i)}\right) = \left\| \overrightarrow{x^{(i)}} - \mathbf{H}^{(i)} \overrightarrow{b} \right\|^2 \quad (28)$$

is the error to be minimized. Minimization of $e^{(i)}(k_I^{(i)}, k_O^{(i)})$ is performed by a standard method of nonlinear minimization where $k_I^{(i)}$ and $k_O^{(i)}$ are varied (see next section).

V. Implementation

The algorithms described above were implemented and tested independently in Matlab and in C++. Relatively standard methods of nonlinear minimization were used for minimizations in CR, IQML and KBI. The L-BFGS-B algorithm [13] (from http://www.netlib.org) which is a modification of the well-known BFGS (Broyden–Fletcher–Goldfarb–Shanno) [14] was used in the case of C++. The function `constr` was used in the case of Matlab. `constr` is an implementation of sequential quadratic programming nonlinear minimization algorithm [15] in Matlab 5.2.

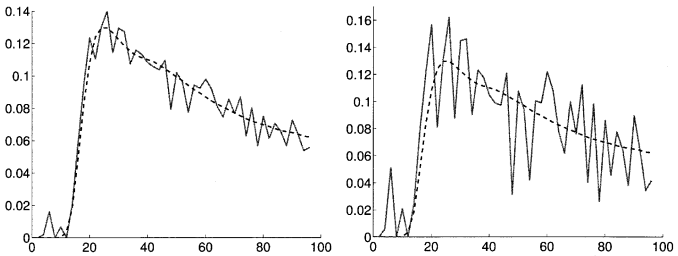

Fig. 3. Examples of tissue time concentration curve [noisy (solid line) and without noise (dashed line)] simulated using blood input function (concentration in mmol/L versus time in seconds) and $k_I = 0.55$ (min^{-1}), $k_O = 3.06$ (min^{-1}). (a) $\sigma_{\mathrm{Noise}} = 0.01$ (mmol/L), (b) $\sigma_{\mathrm{Noise}} = 0.032$ (mmol/L).

Gradients of the minimization cost functions (7) and (14) relative to $k_I^{(i)}$ and $k_O^{(i)}$ were calculated analytically for use in the minimization algorithms which reduced calculation time. The gradients are given in the Appendix-C. Also, for speed the conjugate gradient method and fast Fourier transform were used to reach the linear system solutions $\overrightarrow{\tilde{b}}$ in (13). That is, the linear system $\mathbf{A}\overrightarrow{\tilde{b}} = \overrightarrow{c}$ where $\mathbf{A} = \tilde{\mathbf{H}}^T\tilde{\mathbf{H}}$ and $\overrightarrow{c} = \tilde{\mathbf{H}}^T\overrightarrow{\mathrm{TCs}}$ can be solved for $\overrightarrow{\tilde{b}}$ by the conjugate gradient (CG) method [14]. CG uses multiplication of matrix $\mathbf{A}$ by a vector in each iteration. $\mathbf{A}$ can also be represented as $\mathbf{A} = \sum_{i=1}^{p} \tilde{\mathbf{H}}^{(i)T}\tilde{\mathbf{H}}^{(i)}$. Since multiplication of $N \times N$ matrix $\tilde{\mathbf{H}}^{(i)}$ [built from $h^{(i)}(n)$] by some vector $v(n)$ represents the first N values of convolution of vectors $h^{(i)}$ and v, multiplication of matrix $\tilde{\mathbf{H}}^{(i)T}\tilde{\mathbf{H}}^{(i)}$ by a vector was implemented using element-by-element multiplication of $h^{(i)}$ and v in the Fourier domain.

During the cost function minimizations in CR, IQML, and KBI the values of k_I and k_O were bounded to physically possible ranges. It is important to set up these boundaries (at least for k_O) because at the noise levels used here it strongly influences the accuracy of k_O estimates.

In the EVAM implementation, the eigenvectors were calculated using singular value decomposition (SVD) [14].

VI. Simulations

To evaluate the accuracy of the methods, parameter estimates from simulated MRI TCs for a four channel case (four ROIs) and a two channel case (two ROIs) were made. TCs data were simulated by convolving regional tissue responses with a dynamic contrast MRI blood input function and then adding white Gaussian noise (mean = 0, σ_{Noise} are given below). The blood input function was derived from the $1/T_1(t)$ data presented in [1, Fig. 2] by the formula

$$b(t) = (1/T_1(t) - 1/T_{1\mathrm{initial}})/R \quad (29)$$

where R is the relaxivity constant ($R = 4.8$ (mmol/L $\cdot$ s)$^{-1}$ [16]) and $1/T_{1\mathrm{initial}} = 0.8\,(\mathrm{s}^{-1})$ [1]. 49 time frames were used. The time interval between frames was 2 seconds. An example of one of the TCs with simulated noise and without noise is shown in Fig. 3.

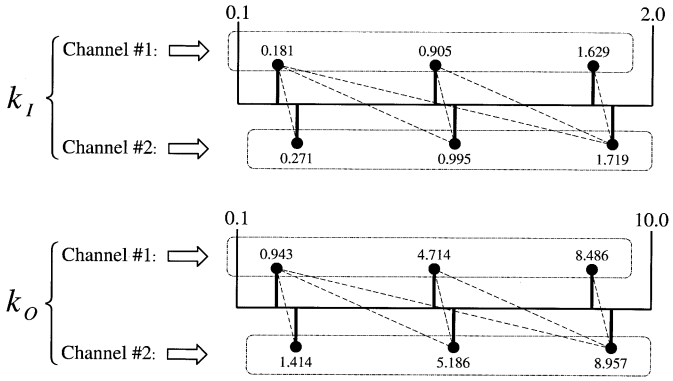

Fig. 4. Physical ranges of kinetic parameters for dynamic cardiac MRI. Numbers near the circles are the values of kinetic parameters that were used in this work for the two channel case. The combinations of parameters of the first channel with parameters of the second channel used in the simulations are denoted by the dashed lines.

Values of $k_I^{(i)}$ and $k_O^{(i)}$ were estimated from each noise realization of TCs by the three algorithms. Estimated values of the kinetic parameters were accumulated into histograms and normalized to sum to one to visualize the bias and variance of the parameters.

During the cost function minimization the values of k_I and k_O were bounded to physiological ranges [between 0.10 and 2.00 (min^{-1}) for k_I and between 0.10 and 10.00 (min^{-1}) for k_O (based on data in [17]–[19])].

To compare the performance of the blind identification methods with conventional techniques under the same conditions, kinetic parameters from the same sample of simulated noisy TCs were estimated with knowledge of the blood input function (KBI). The comparisons were made for the best performance possible by the conventional techniques—it was assumed that the blood input was known exactly without any noise. However, some noise is always present in real measurements of the blood input.

A. Four Channel Case

The coefficients for the regions $k_I^{(1)}, k_I^{(2)}, k_I^{(3)}, k_I^{(4)}$, were set to 0.55, 1.37, 1.07, 0.90 (min^{-1}) and $k_O^{(1)}, k_O^{(2)}, k_O^{(3)}, k_O^{(4)}$, were set to 3.06, 9.13, 6.69, 3.00 (min^{-1}) (values within expected physiological ranges for tissue kinetic parameters in myocardial perfusion MRI).

Ten-thousand noise realizations of the TCs were generated at $\sigma_{\mathrm{Noise}} = 0.01$ (mmol/L) and $\sigma_{\mathrm{Noise}} = 0.032$ (mmol/L). (variance $= 0.001$ and 0.01, respectively).

B. Two Channel Case

Thirty-six different combinations of the parameters k_I and k_O for two channels were used to evaluate the performance of the algorithms. The combinations of the true parameters used and physical ranges for k_I and k_O are shown in Fig. 4.

Estimation of k_O and $k_I^{(2)}/k_I^{(1)}$ ratios for these combinations were performed using noisy TCs at the noise level $\sigma_{\mathrm{Noise}} = 0.01$ (mmol/L).

The probability density functions (PDFs) (normalized histograms) were obtained from distributions of estimates performed for 10 000 noisy TCs' realizations.

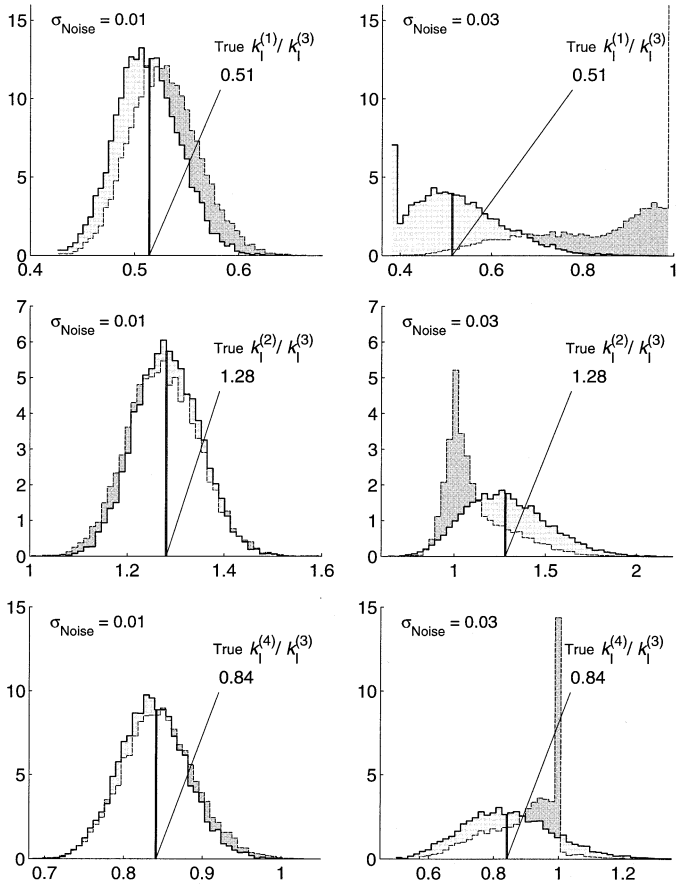

Fig. 5. PDF of the ratio $k_I^{(i)}/k_I^{(3)}$ estimates by IQML (solid) and by CR (dash) methods computed from simulated noisy TCs.

VII. Results

A. Four Channel Case

The PDFs of $k_O^{(i)}$ and the ratios $k_I^{(i)}/k_I^{(3)}$ estimated by CR and IQML methods are shown in Figs. 5 and 6.

The mean and standard deviation were evaluated from these distributions (Tables I–IV). It can be seen from the figures that the IQML method has significantly less bias than CR (especially in the higher noise case of $\sigma_{\mathrm{Noise}} = 0.032$) and smaller standard deviation.

Also, k_O was estimated for the case of low noise ($\sigma_{\mathrm{Noise}} = 0.01$) using the EVAM algorithm (multichannel case described in the Appendix). The mean and standard deviation are shown in Table III. It can be seen from the table that the efficiency of EVAM is much worse than CR or IQML.

Comparing IQML and KBI in k_O, we see significantly better accuracy for KBI versus IQML (Tables III, IV). On the other hand looking at the ratios $k_I^{(i)}/k_I^{(3)}$ it can be seen (from Tables I and II) that the performance of IQML is not far from KBI (especially at low noise $\sigma_{\mathrm{Noise}} = 0.01$).

B. Two Channel Case

The mean and standard deviation of the parameter estimates for the two channel case are shown in Fig. 8. In some cases, there were no clear peaks—the algorithms essentially failed under these conditions. These cases are denoted by an $\times$ in the diagram. There are footnotes in the diagram regarding the nature

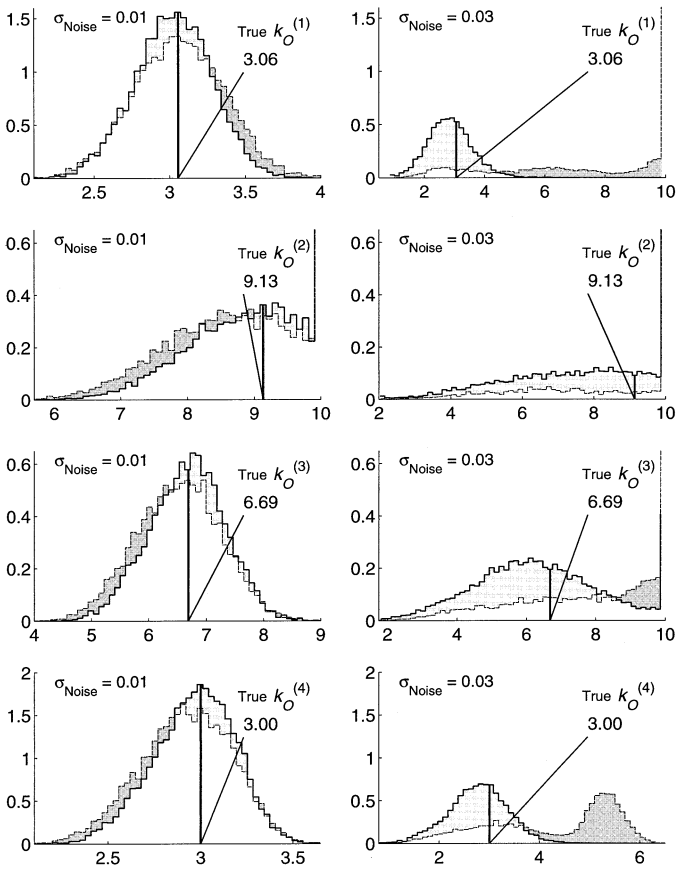

Fig. 6. PDF of k_O estimates by IQML (solid) and by CR (dash) methods computed from simulated noisy TCs.

TABLE I
$k_I^{(i)}/k_I^{(3)}$ RATIOS ($\sigma_{\text{noise}} = 0.01$ IN TISSUE CONCENTRATION CURVES)

$\sigma_N =$	$k_I^{(1)}/k_I^{(3)}$		$k_I^{(2)}/k_I^{(3)}$		$k_I^{(4)}/k_I^{(3)}$	
0.01	mean	std	mean	std	mean	std
IQML	0.512	0.030	1.283	0.067	0.837	0.043
CR	0.528	0.033	1.274	0.074	0.845	0.047
KBI	0.514	0.028	1.281	0.066	0.842	0.037
true	0.514		1.280		0.841	

TABLE II
$k_I^{(i)}/k_I^{(3)}$ RATIOS ($\sigma_{\text{noise}} = 0.032$ IN TISSUE CONCENTRATION CURVES)

$\sigma_N =$	$k_I^{(1)}/k_I^{(3)}$		$k_I^{(2)}/k_I^{(3)}$		$k_I^{(4)}/k_I^{(3)}$	
0.03	mean	std	mean	std	mean	std
IQML	0.522	0.101	1.284	0.227	0.848	0.141
CR	0.854	0.148	1.110	0.177	0.901	0.110
KBI	0.521	0.090	1.272	0.192	0.849	0.120
true	0.514		1.280		0.841	

of PDF distributions of the parameter estimates. These footnotes call attention to distributions that contain clear peaks but are not completely in a Gaussian-like shape. From Fig. 8, it can be noticed again that the IQML, in many cases, gives better estimates than CR.

Also, it is possible to see from the diagram that blind identification algorithms are more stable in the estimation of the ratios

TABLE III
$k_O^{(i)}$ ($\sigma_{\text{noise}} = 0.01$ IN TISSUE CONCENTRATION CURVES)

$\sigma_N =$	$k_O^{(1)}$		$k_O^{(2)}$		$k_O^{(3)}$		$k_O^{(4)}$	
0.01	mean	std	mean	std	mean	std	mean	std
IQML	3.02	0.26	9.10	0.87	6.66	0.66	2.96	0.22
CR	3.06	0.30	8.81	0.99	6.51	0.73	2.92	0.25
KBI	3.06	0.15	9.14	0.41	6.70	0.30	3.00	0.09
EVAM	3.08	1.21	7.95	2.48	6.68	2.75	3.07	1.39
true	3.06		9.13		6.69		3.00	

TABLE IV
$k_O^{(i)}$ ($\sigma_{\text{noise}} = 0.032$ IN TISSUE CONCENTRATION CURVES)

$\sigma_N =$	$k_O^{(1)}$		$k_O^{(2)}$		$k_O^{(3)}$		$k_O^{(4)}$	
0.03	mean	std	mean	std	mean	std	mean	std
IQML	2.85	0.74	8.45	1.95	6.36	1.82	2.77	0.61
CR	7.57	2.77	9.43	1.43	8.53	1.97	4.25	1.27
KBI	3.09	0.49	8.97	0.97	6.76	0.98	3.01	0.30
true	3.06		9.13		6.69		3.00	

$k_I^{(2)}/k_I^{(1)}$ than in the estimation of k_O. It can be seen that they give in many cases good accuracy of $k_I^{(2)}/k_I^{(1)}$ estimates when estimation of k_O is failing or has poor accuracy.

VIII. REAL DATA CASE

A normal volunteer was imaged with MRI in a manner similar to that in [18] with a high Gd dose. Two nonadjacent regions and a blood input region were traced on a mid-ventricular slice. This blood input measurement is inaccurate because of the nonlinear relationship between signal and concentration at high Gd concentrations. Comparison of blind estimation by IQML with estimation by KBI using the inaccurate measured blood input was performed. The last two time points of the measured blood input were assumed to be close to the true values since they have relatively low Gd concentrations. Therefore, during the IQML estimation the last two points of the blood input vector were fixed to the values of the last two points of the measured blood. This is a way to obtain absolute values of k_I by IQML.

Fig. 7(a) shows the blood input function estimated by IQML and the measured blood input. Fig. 7(b) shows the two measured TCs and their fits by IQML and KBI. It can be seen that the fit of TCs is better with IQML ($\chi^2_{\text{fit}} = 4.0 \cdot 10^{-4}$) than is the fit with KBI ($\chi^2_{\text{fit}} = 4.1 \cdot 10^{-3}$).

Blind estimation by IQML performed on the two measured TCs gave: $k_I = [2.65, 1.57]$, $k_O = [5.84, 4.64]$. Estimates using the measured blood input were: $k_I = [4.14, 2.48]$, $k_O = [11.15, 8.93]$. At lower Gd doses [which entail a lower signal-to-noise ratio (SNR)], KBI is expected to give correct parameter estimates. In this high-Gd dose example with realdata, IQML gives much more reasonable estimates of k_I and k_O [typical ranges for k_I and k_O were given above (Section VI)] than KBI with blood input measured from images. Future work will involve animal studies with a microsphere based gold standard of flow to validate the blind methods.

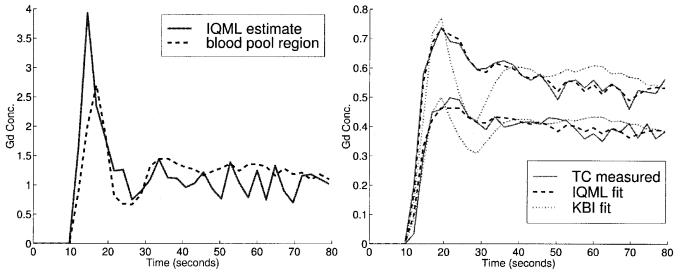

(a) (b)

Fig. 7. (a) Blood input estimate by IQML (solid), blood input measured from blood pool region (dash). (b) Two measured tissue time concentration curves (solid), fit resulted from blind estimation by IQML (dash), fit by KBI using blood input measured from blood pool region.

IX. Discussion

The ability to accurately determine kinetic parameters without the use of an input function would be extremely valuable in a large number of medical imaging applications. This work compared three methods and analyzed their accuracy in noise. The blind identification methods were shown to be sensitive to noise but potentially useful in practice for estimation of uptake ratios; the accuracy of IQML was shown to be very close to that of using an ideal noise-free input function (KBI) in many cases. On the other hand, estimation of the washout parameters using blind identification may not be viable with these methods when the tissue concentration curves are fairly noisy.

The IQML method gives more accurate estimates than the other blind identification methods presented. The CR method is comparable to the IQML but is less stable and in some cases shows two peaks instead of one (Fig. 6). EVAM gives relatively poor estimates.

From Fig. 8, two effects can be noted. One is that the accuracy of the $k_O^{(1)}$ estimates deteriorates when values of the true $k_O^{(1)}$ and $k_O^{(2)}$ parameters are close to each other (see especially bottom left corner of Fig. 8). This happens because the convolution matrix $\mathbf{H}$ is close to singular; in other words, the poles of the channel transfer functions are close to each other so the identification of the channels is difficult in the presence of noise. Another and more useful effect is that despite of inaccurate k_O estimates the $k_I^{(2)}/k_I^{(1)}$ estimation can still provide accurate results. Relative measures of flow have been shown to be valuable clinically in SPECT and MRI [20]. Absolute values of flow-related parameters such as k_I may be even more useful clinically. Such information may be obtained for example by combining the blind approach with a blood sample from an artery or from a late MRI time image where it is known that error due to artifacts is minimal, (as was done in Section VIII).

The results show that the accuracy of all of the methods improves with increases in k_I because the SNR increases in TCs with larger k_I. This trend is particularly noticable in the right-hand side of Fig. 8; the upper three boxes show relatively poor results due to the low SNR of the $k_I^{(1)} = 0.18$ curve while the lower three boxes with high SNRs give excellent results.

An important issue that has been noted from the simulations is that the appropriate choice of the boundaries for the estimated k_O is essential because of its influence on the accuracy of estimates. The estimations were also performed with a different set of boundaries and deterioration of the accuracy for k_O was observed when the boundaries did not correspond to the physical ranges of the coefficients.

Some limitations of this work should be noted. The fraction of the blood f_v [2] in the tissue region due to the capillaries throughout the tissue or from partial volume effects was not modeled. The simulations here did not take into account artifacts such as motion or other possible errors in the measured tissue concentration curves. Such artifacts are application dependent and would be important to consider when applying these methods to real data.

Gaussian noise was used in these simulations. For emission tomography, Poisson noise would be a more appropriate model. Appropriate weightings of the error functions would then be more complex.

X. Conclusion

Computer simulations using a physiologically realistic two-compartment model and additive Gaussian noise showed that the IQML method gives more accurate kinetic parameter estimates than the CR method or EVAM.

The IQML blind parameter estimation method is likely accurate enough in its current state to benefit some medical imaging applications in which uptake ratios are needed. It is probable that incorporation of *a priori* information about the blood input will give better accuracy for blind estimations. Future work will involve development of appropriate *a priori* information for specific applications and further comparison of various methods for blind estimation with real data.

Appendix

A. Proof of Uniqueness

Assuming $B^{(i)} = \Delta t \cdot k_I^{(i)}$ and $\lambda^{(i)} = \Delta t \cdot k_O^{(i)}$, (4) can be written as

$$h^{(i)}(n) = B^{(i)} \cdot e^{-\lambda^{(i)} \cdot n}. \tag{30}$$

The transfer function for channel i is

$$\mathcal{H}^{(i)}(z^{-1}) = \frac{B^{(i)}}{1 - e^{-\lambda^{(i)}} z^{-1}}. \tag{31}$$

According to (31), in the physiological two-compartment model case the order of the FIR filters of the blind deconvolution adaptive system (note the impulse responses of the compartment models are IIR) is known and is equal for all of the channels: $W^{(i)} = 1$ $(i = 1, \ldots, p)$ where $W^{(i)}$ is the order of the ith FIR filter and i is the channel number. Then, the FIR filters of the blind deconvolution adaptive system can be written as

$$\mathcal{W}^{(i)}(z^{-1}) = w_0^{(i)} + w_1^{(i)} z^{-1}, \qquad i = 1, \ldots, p \tag{32}$$

where $w_0^{(i)}$ and $w_1^{(i)}$ are the coefficients of the FIR filter for the channel number i. According to [5] and (31), the unique solutions for FIR filters of blind deconvolution adaptive system for the two-channel case are

$$\mathcal{W}^{(1)}(z^{-1}) = \alpha \left(1 - e^{-\lambda^{(1)}} z^{-1}\right) B^{(2)} \tag{33}$$

$$\mathcal{W}^{(2)}(z^{-1}) = \alpha \left(1 - e^{-\lambda^{(2)}} z^{-1}\right) B^{(1)} \tag{34}$$

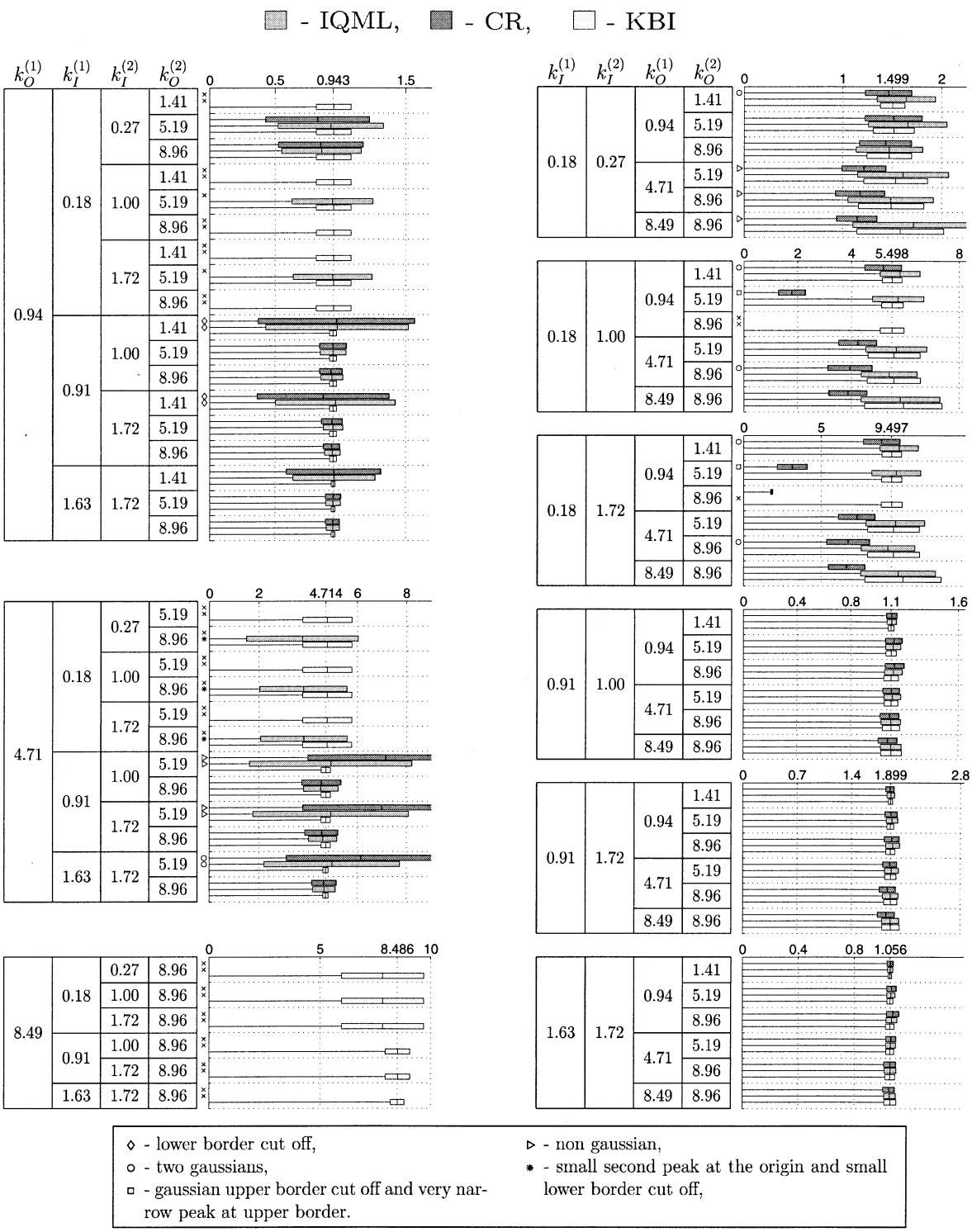

Fig. 8. Two channel case estimates of $k_O^{(1)}$ (left column) and of the ratio $k_I^{(2)}/k_I^{(1)}$ (right column). Mean and $\pm$ standard deviation calculated from the PDFs are shown in comparison for CR, IQML, and KBI. ($\sigma_{\text{noise}} = 0.01$ in tissue concentration curves). In some cases, there were no clear peaks in the distributions—the algorithms essentially failed under these conditions. These cases are denoted by an $\times$ sign. The footnotes regard the nature of PDF distributions of the parameter estimates and indicate distributions that contain clear peaks but are not completely in a Gaussian-like shape.

where α is an arbitrary constant. Using the expressions for the filters (33) and (34), it can be seen that the coefficients of the FIR filters are

$$w_0^{(1)} = \alpha B^{(2)}, \qquad w_1^{(1)} = -\alpha B^{(2)} e^{-\lambda^{(1)}} \tag{35}$$

$$w_0^{(2)} = \alpha B^{(1)}, \qquad w_1^{(2)} = -\alpha B^{(1)} e^{-\lambda^{(2)}}. \tag{36}$$

The FIR coefficients $w_0^{(1)}$, $w_1^{(1)}$, $w_0^{(2)}$ and $w_1^{(2)}$ correspond to the eigenvector for the minimal eigenvalue of matrix $\mathbf{R}$ *sample correlation matrix* defined in [5] and in (26). They can be found

uniquely by SVD or other decompositions. Therefore, k_I can be found within a scale factor and k_O can be found exactly

$$k_I^{(1)} \Big/ k_I^{(2)} = w_0^{(2)} \Big/ w_0^{(1)} \tag{37}$$

$$k_O^{(i)} = -\ln\left(-w_1^{(i)} \Big/ w_0^{(i)}\right) \Big/ \Delta t. \tag{38}$$

Thus, the problem of finding kinetic parameters for this kind of tissue response has a unique solution. Uniqueness in the two channel problem implies uniqueness in the multichannel case because all possible pairwise combinations in the set of multichannels will yield unique solutions.

While we have shown with EVAM that the blind estimation problem has a unique solution, this does not constitute a proof that IQML and CR converge to the unique solution. However, the simulations indicate IQML and CR are robust methods for convergence to the unique solution.

B. Short Description of EVAM for Multichannels

This multichannel description is valid only when the transfer functions of the channels are all poles or all zeros. Here the orders of transfer functions for all of the channels are assumed to be the same and known; the more general case is described in [5].

In the multichannel case, we need to consider each combination of two different channels. Using the same definitions as in (20), the error signal $e_{i,j}(n)$ for each pair of the channels i and j in this case will be

$$e_{i,j}(n) = y^{(i)}(n) - y^{(j)}(n) \tag{39}$$

or

$$e_{i,j}(n) = [\mathbf{w}^{(i)T} \quad \mathbf{w}^{(j)T}] \begin{bmatrix} \mathbf{x}^{(i)}(n) \\ -\mathbf{x}^{(j)}(n) \end{bmatrix}. \tag{40}$$

The mean square error can be defined as

$$\mathcal{E}(\mathbf{w}) = \sum_{n=M}^{N} \sum_{i=1}^{p-1} \sum_{j=i+1}^{p} |e_{i,j}(n)|^2 \tag{41}$$

and the vector $\mathbf{w}$ redefined for the general case of p channels as

$$\mathbf{w} = \left[\mathbf{w}^{(1)T}, \mathbf{w}^{(2)T}, \ldots, \mathbf{w}^{(p)T}\right]^T \tag{42}$$

then

$$\mathcal{E}(\mathbf{w}) = \mathbf{w}^T \mathbf{R} \mathbf{w} \tag{43}$$

where, using the same block matrix definition as in (27), matrix $\mathbf{R}$ is equal to

$$\begin{bmatrix} s\mathbf{R}_{1,1} & -\mathbf{R}_{1,2} & \cdots & -\mathbf{R}_{1,p} \\ -\mathbf{R}_{2,1} & s\mathbf{R}_{2,2} & \ddots & \vdots \\ \vdots & \ddots & \ddots & -\mathbf{R}_{p-1,p} \\ -\mathbf{R}_{p,1} & \cdots & -\mathbf{R}_{p,p-1} & s\mathbf{R}_{p,p} \end{bmatrix} \tag{44}$$

and

$$s = p - 1.$$

Again, the $\mathbf{w}$ which minimizes $\mathcal{E}(\mathbf{w})$ is the eigenvector of $\mathbf{R}$ that corresponds to the minimal eigenvalue.

C. Gradients of Objective Function

For use below, the partial derivatives of the tissue response in (4) are

$$\frac{\partial h^{(i)}(n)}{\partial k_I^{(i)}} = \frac{h^{(i)}(n)}{k_I^{(i)}}, \quad \frac{\partial h^{(i)}(n)}{\partial k_O^{(i)}} = -n \cdot \Delta t \cdot h^{(i)}(n). \tag{45}$$

1) In CR: Denoting the convolution of the measured data for channel i with the tissue response for channel j [$h^{(j)}(n)$ where $n = 0, \ldots, N-1$] as

$$S_a^{(i,j)} = x^{(i)} \otimes h^{(j)} = \sum_{n=0}^{a} x^{(i)}(a-n) h^{(j)}(n) \tag{46}$$

and also denoting $(S_a^{(i,j)} - S_a^{(j,i)})$ as $d_a^{(i,j)}$ and $\sum_{a=0}^{N-1} (d_a^{(i,j)})^2$ as $v^{(i,j)}$, the objective function (7) (denoted as R) can be expressed as

$$R = \sum_{i=1}^{p-1} \sum_{j=i+1}^{p} v^{(i,j)}. \tag{47}$$

The gradient of R by parameter $k^{(m)}$ (where k is either k_I or k_O) of channel m for $m = 1, \ldots, p$

$$\partial R / \partial k^{(m)} = \sum_{j=m+1}^{p} \frac{\partial v^{(m,j)}}{\partial k^{(m)}} + \sum_{i=1}^{m-1} \frac{\partial v^{(i,m)}}{\partial k^{(m)}} \tag{48}$$

where the partial derivatives are

$$\frac{\partial v^{(i,j)}}{\partial k^{(i)}} = 2 \sum_{a=0}^{N-1} d_a^{(i,j)} \left(0 - \sum_{n=0}^{a} x^{(j)}(a-n) \frac{\partial h^{(i)}(n)}{\partial k^{(i)}}\right) \tag{49}$$

and

$$\frac{\partial v^{(i,j)}}{\partial k^{(j)}} = 2 \sum_{a=0}^{N-1} d_a^{(i,j)} \left(\sum_{n=0}^{a} x^{(i)}(a-n) \frac{\partial h^{(j)}(n)}{\partial k^{(j)}} - 0\right). \tag{50}$$

2) In IQML: Gradients of the objective function (14) are

$$\partial R / \partial k^{(m)} = 2 \left[\left(\tilde{\mathbf{H}} \tilde{\mathbf{H}}^{\dagger} - \mathbf{I}\right) \overrightarrow{\mathrm{TCs}}\right]^T \left(\partial \tilde{\mathbf{H}} / \partial k^{(m)}\right) \tilde{\mathbf{H}}^{\dagger} \overrightarrow{\mathrm{TCs}} \tag{51}$$

where $\partial \tilde{\mathbf{H}} / \partial k^{(m)}$ is a matrix each element of which is equal to the derivative of the correspondent element of $\tilde{\mathbf{H}}$ by $k^{(m)}$. A rigorous proof can be found in [10]. Relation (51) also is equivalent to

$$\partial R / \partial k^{(m)} = 2 \left(\tilde{\mathbf{H}} \overrightarrow{\tilde{b}} - \overrightarrow{\mathrm{TCs}}\right)^T \left(\partial \tilde{\mathbf{H}} / \partial k^{(m)}\right) \overrightarrow{\tilde{b}} \tag{52}$$

which was used in the code.

Acknowledgment

The authors would like to thank Dr. B. Bromley for very useful discussions.

References

[1] J.-P. Vallee, H. D. Sostman, J. R. MacFall, T. Wheeler, L. W. Hedlund, C. E. Spritzer, and R. E. Coleman, "MRI quantitative myocardial perfusion with compartmental analysis: A rest and stress study," *Magn. Reson. Med.*, vol. 38, pp. 981–989, 1997.

[2] E. V. R. Di Bella, R. Clackdoyle, and G. T. Gullberg, "Blind estimation of compartmental model parameters," *Phys. Med. Biol.*, vol. 44, pp. 765–780, 1999.
[3] K. Chen, D. Bandy, E. Reiman, S.-C. Huang, M. Lawson, D. Feng, L. Yun, and A. Palant, "Noninvasive quantification of the cerebral metabolic rate for glucose using positron emission tomography^{18}F–Fluoro–2–Deoxyglucose, the Patlak method, and an image derived input function," *J. Cereb. Blood Flow Metab.*, vol. 18, no. 7, pp. 716–723, 1998.
[4] S. Takikawa, V. Dhawan, P. Spetsieres, W. Robeson, T. Chaly, R. Dahl, D. Margouleff, and D. Eidelberg, "Noninvasive quantitative fluorodeoxyglucose PET studies with an estimated input function derived from a population-based arterial blood curve," *Radiology*, vol. 188, no. 1, pp. 131–136, 1993.
[5] M. I. Gürelli and C. L. Nikias, "EVAM: An eigenvector-based algorithm for multichannel blind deconvolution of input colored signals," *IEEE Trans. Signal Processing*, vol. 43, pp. 134–149, Jan. 1995.
[6] C.-H. Lau, P.-K. D. Lun, and D. Feng, "Non-invasive quantification of physiological processes with dynamic PET using blind deconvolution," in *Proc. Int. Conf. Acoustics, Speech and Signal Processing*, vol. 3, Seattle, WA, 1998, pp. 1805–1808.
[7] R. E. Carson, Y. Yan, and R. Shrager, "Absolute cerebral blood flow with [^{15}O] water and PET. Determination without measured input function," in *Cerebral Blood Flow Imaging Conf.* Bethesda, MD: Academic, 1996, pp. 185–195.
[8] K.-P. Wong, D. Feng, S. R. Meikle, and M. J. Fulham, "Simultaneous estimation of physiological parameters and the input function—*In vivo* PET data," *IEEE Trans. Inform. Technol. Biomed.*, vol. 5, pp. 67–76, Mar. 2001.
[9] D. Feng, K.-P. Wong, C.-M. Wu, and W. C. Siu, "A technique for extracting physiological parameters and the required input function simultaneously from PET image measurements: Theory and simulation study," *IEEE Trans. Inform. Technol. Biomed.*, vol. 1, pp. 243–254, Dec. 1997.
[10] G. H. Golub and V. Pereyra, "The differentiation of pseudo-inverses and nonlinear least squares problems whose variables separate," *SIAM J. Numer. Anal.*, vol. 10, no. 2, pp. 413–432, April 1973.
[11] L. Tong and S. Perreau, "Multichannel blind identification: From subspace to maximum likelihood methods," *Proc. IEEE*, vol. 86, no. 10, pp. 1951–1968, Oct. 1998.
[12] Y. Bresler and A. Macovski, "Exact maximum likelihood parameter estimation of superimposed exponential signals in noise," *IEEE Trans. Acoust., Speech Signal Processing*, vol. ASSP-34, pp. 1081–1089, Oct. 1986.
[13] R. H. Byrd, P. Lu, J. Nocedal, and C. Zhu, "A limited memory algorithm for bound constrained optimization," *SIAM J. Scientific Computing*, vol. 16, no. 5, pp. 1190–1208, 1995.
[14] W. H. Press, S. F. Teukolsky, W. T. Vetterling, and B. P. Flannery, *Numerical Recipes in C: the Art of Scientific Computing*, 2nd ed. Cambridge, U.K.: Cambridge University Press, 1992.
[15] *Matlab Optimization Toolbox User's Guide version 5*, The MathWorks, Natick, MA, 1997.
[16] K. M. Donahue, D. Burstein, M. L. Gray, and W. J. Manning, "Studies of Gd-DTPA relaxivity and proton exchange rates in tissue," *Magn. Reson. Med.*, pp. 66–76, 1994.
[17] N. Wilke, M. Jerosch-Herold, Y. Wang, Y. Huang, B. V. Christensen, A. E. Stilllman, K. Ugurbil, K. McDonald, and R. F. Wilson, "Myocardial perfusion reserve: Assessment with multisection, quantitative, first-pass MR imaging," *Radiology*, vol. 204, pp. 373–384, 1997.
[18] J.-P. Vallee, F. Lazeyras, L. Kasuboski, P. Chatelain, N. Howarth, A. Righetti, and D. Didier, "Quantification of myocardial perfusion with FAST sequence and GdBolus in patients with normal cardiac function," *J. Magn. Reson. Imag.*, vol. 9, pp. 197–203, 1999.
[19] J.-P. Vallee, H. D. Sostman, J. R. MacFall, T. R. DeGrado, J. Zhang, L. Sebbag, F. R. Cobb, T. Wheeler, L. W. Hedlund, T. G. Turkington, C. E. Spritzer, and R. E. Coleman, "Quantification of myocardial perfusion by MRI after coronary occlusion," *Magn. Reson. Med.*, vol. 40, pp. 287–297, 1998.
[20] N. Al-Saadi, E. Nagel, M. Gross, A. Bornstedt, B. Schnackenburg, C. Klein, W. Klimek, H. Oswald, and E. Fleck, "Noninvasive detection of myocardial ischemia from perfusion reserve based on cardiovascular magnetic resonance," *Circulation*, vol. 101, pp. 1379–1383, 2000.

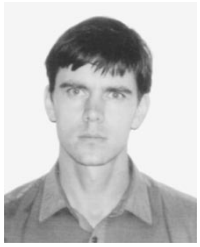

Dmitri Y. Riabkov received the Diploma degree in physics from Moscow Engineering Physics Institute, Moscow, Russia, in 1994. He is working towards the Ph.D. degree in medical physics and he is doing research at the Medical Imaging Research Laboratory at the University of Utah, Salt Lake City.

He was a Researcher at the Joint Institute of Nuclear Physics, Dubna, Russia, from 1994 to 1998. His research interests include development and analysis of algorithms in dynamic medical imaging.

Edward V. R. Di Bella received the B.S. degree in electrical engineering from the University of Virginia, Charlottesville, in 1988 and the M.S. degree in biomedical engineering from the University of Vermont, Burlington, in 1991, and the Ph.D. degree from the Georgia Institute of Technology, Atlanta, in 1995.

Since 1995, he has been at the University of Utah. He is currently an Assistant Professor in the Medical Imaging Research Laboratory in the Department of Radiology at the University of Utah. His research interests include model-based quantitative imaging of flow and metabolism, and automated methods of image analysis.